Proceedings of the ASME 2016 International Mechanical Engineering Congress & Exposition
IMECE16
November 11-17, 2016, Phoenix, Arizona, USA

IMECE2016-67013

TEMPERATURE-STAGED THERMAL ENERGY STORAGE ENABLING LOW THERMAL EXERGY LOSS REFLUX BOILING IN FULL SPECTRUM SOLAR SYSTEMS

Terry J. Hendricks, Bill J. Nesmith, Jonathan Grandidier
Power and Sensors Section, Thermal Energy Conversion Applications & Systems
NASA-Jet Propulsion Laboratory, California Institute of Technology
Pasadena, California, USA

ABSTRACT

Hybrid full spectrum solar systems (FSSS) designed to capture and convert the full solar wavelength spectrum use hybrid solar photovoltaic/thermodynamic cycles that require low thermal exergy loss systems capable of transferring high thermal energy rates and fluxes with very low temperature differentials and losses. One approach to achieving this capability are high-heat-flux reflux boiling systems that take advantage of high heat transfer boiling and condensation mechanisms. Advanced solar systems are also intermittent by their nature and their electrical generation is often out-of-phase with electric utility power demand, and their required power system cycling reduces efficiency, performance (dispatchability), lifetime, and reliability. High temperature thermal energy storage (TES) at 300-600°C enables these reflux boiling systems to simultaneously store thermal energy internally to increase the energy dispatchability of the associated solar system, as this can increase the power generation profile by several hours (up to 6-10 hours) per day. Many TES phase change materials (PCM's) exist including KNO_3, $NaNO_3$, LiBr/KBr, $MgCl_2$/NaCl/KCl, Zn/Mg, and CuCl/NaCl, which have various operating melting points and different latent heats of fusion. Common, cost effective TES PCM's are $FeCl_2$/NaCl/KCl mixtures, whose phase change temperature can be varied and controlled by simple composition adjustments. This paper presents and discusses unique "temperature-staged" thermal energy storage configurations using these TES materials and analysis of such systems integrated into high-heat-flux reflux boiling systems. In this specific application, the TES materials are designed to operate at staged temperatures surrounding an operating design point near 350°C, while providing 18 kW of source heat transfer to operate a thermoacoustic power system during off-sun conditions (e.g., temporary cloud conditions, after sun-down). This work discusses relevant configurations, and critical thermal and entropy models of the TES configurations, which show the inherent minimization of thermal exergy during critical heat transfers within the configurations and systems envisioned.

NOMENCLATURE

English

a – 1st system design parameter in Eq. 1
b – 2nd system design parameter in Eq. 1
A_{HT} – Heat transfer area of TES material surface [m^2]
$A_{s,c}$ – Heat transfer area on outside of storage chamber [m^2]
C_p – TES or Naphthalene heat capacity [J/kg-K]
E_g – Internal energy generation [W]
E_{st} – Internal energy storage (sink) [W]
h_s – Thermal convection coefficient on outside of storage chamber [W/m^2-K]
$h_{lat,TES}$ – TES Latent heat of fusion or latent energy of fusion [kJ/kg or J/g]
$\bar{h}$ - Heat transfer coefficient at the TES surfaces [W/m^2-K]
m – Mass of system constituents (TES or naphthalene) – [kg]
t – time (seconds and hours)
S_f – Final entropy state [J/K]
S_i – Initial entropy state [J/K]
S_{gen} – Entropy generation [J/K]
$S_{gen,total}$ – Total entropy generation [J/K]
$S_{gen,HT}$ – Entropy generation [J/K]
T_∞ - Temperature at $t \rightarrow \infty$ [K]
T_{amb} – Ambient environment temperature outside the storage chamber [K]
T_f – Final internal storage temperature during charging [K]
T_i – Initial internal storage temperature during charging [K]

California Institute of Technology. U.S. Government sponsorship acknowledged.

T_{int} – Lumped, combined internal temperature of storage medium [K]
T_{TES} - Thermal Energy Storage medium phase change temperature [K]
q_s , q_{solar} – Solar flux input [W/m^2]
q_{rad} – Thermal radiation from storage chamber to outside ambient environment [W/m^2]
q_{conv} – Thermal convection from storage chamber to outside ambient environment [W/m^2]
V – Reflux chamber volume [m^3]

Greek
$\Delta T_{Naph-TES}$ – Temperature differential between Naphthalene and TES surfaces [K]
ρ – TES density [kg/m^3]
κ - TES thermal conductivity [W/m-K]
$\eta_{frac-Carnot}$ – Fraction of Carnot efficiency during the energy storage/dissipation process

Subscripts
TES – Associated with Thermal Energy Storage materials
Naph – Associated with Naphthalene materials

INTRODUCTION

Concentrating solar power (CSP) is a highly-promising, utility-scale power solution in a global environment with increasing energy demand, limited and more expensive fossil fuel resources, national government incentives worldwide for renewable energy deployment, and growing concerns over the environmental implications of conventional fuel sources like coal, gas, and nuclear fission material. Efficient, low-cost thermal energy storage (TES) enhances concentrated solar power (CSP) systems by increasing their capacity factors, enhancing dispatchability, and lowering levelized costs of electricity (LCOE) [1, 2]. Various researchers, government and industrial programs have investigated the merits and metrics of thermal energy storage in solar power plants [3-9]. Denholm et al. [4] in particular investigated the cost impacts of TES approaches and solutions on CSP systems. Investigations have highlighted the merits and drawbacks of various types of thermal energy storage; sensible thermal storage, phase change thermal storage, and thermochemical storage [9, 10, 11]. The U.S. Department of Energy (DOE), Advanced Research Projects Agency-Energy (ARPA-E) has initiated and sponsored research, through the Full Spectrum Optimized Conversion and Utilization of Sunlight (FOCUS) program, into developing and demonstrating advanced hybrid solar photovoltaic/thermodynamic cycle systems incorporating innovative, exergetically-efficient TES materials and approaches to enhance CSP dispatchability and capacity factors [2]. This work emanates from that FOCUS sponsorship and demonstrates an innovative methodology to incorporate multiple TES materials within a system that minimizes thermal exergy destruction, thereby increasing overall thermal efficiency within the CSP system over sun-on and sun-off operational periods. In particular, this innovative multiple TES material approach attempts to selectively optimize TES materials and storage properties, and the thermal storage configuration integrated within a highly-efficient, low-exergy-loss reflux boiling heat transfer system. This critical heat transfer system transports large amounts of thermal energy between the solar cavity receiver and the thermodynamic cycle power system (in this case a thermoacoustic power converter (TAPC)) within our hybrid solar power system. It also allows a lighter weight, more compact system and a higher performance (lower thermal exergy) system as the point of heat transfer is in direct contact with the working fluid. This system also provides a "thermal switch" feature as the highest temperature TES serves as a safety-enhancing thermal storage point that provides more recovery and reaction time to any undesirable thermal transients emanating from unanticipated equipment failures, process anomalies, or overall cooling losses or disconnections in a hybrid FSSS.

Figure 1 shows a schematic of the hybrid solar power system discussed herein and the integrated reflux boiling/TES sub-system [12]. This system is described in depth by Lee et al. [12]. In general concentrated solar energy is focused from a parabolic dish solar concentrator into the aperture (I1) of a solar receiver cavity (I2) which contains high-temperature (~350°C) concentrator multi-junction solar photovoltaic (MJSPV) cells. The concentrated solar energy is focused by the solar concentrator and aperture system such that it distributes on the high-temperature (HT) MJSPV cells within the solar receiver cavity. A portion of the solar spectrum (generally up to wavelengths of 1.1 to 1.2 μm) is absorbed by the HT MJSPV cells, and the remaining portion of the solar spectrum (infrared wavelengths and longer wavelengths > 1.2μm) is absorbed as thermal energy in the Reflux Boiler Chamber (I3) integrated with TES materials (I5). The Reflux Boiler is designed to absorbed the large thermal loads (~18 kW) via low-thermal-exergy boiling processes and transfer this heat to the hot-head of the TAPC via low-thermal-exergy condensation processes in the TAPC hot-head heat exchanger (I4). The TAPC then converts the incoming thermal energy (which is essentially the initial solar spectrum not converted by the MJSPV cells) by operating between its hot-head heat exchanger (I4) conditions (~350°C) and its cold-

California Institute of Technology. U.S. Government sponsorship acknowledged.

side heat exchanger (I6) conditions (~45°C). The Reflux Boiler is specifically designed to deliver 18kW$_{th}$ (thermal energy) to the TAPC hot-head heat exchanger with approximately 20°C temperature differential between the Reflux Chamber boiling surfaces and the TAPC hot-head heat exchanger surfaces [12]. This work focused on phase change TES materials (I5) and optimizing various system configurations for the Reflux Boiler (I3) and TES materials (I5). Overall system-level objectives for this hybrid system are to demonstrate a total system power output of 10 kW$_e$ with system conversion efficiency of 44% and 15-minutes of TES capability in the first TRL 4-5 prototype. The plan is to ultimately scale the TES capability to provide full system power for 6-10 hours of off-sun- operation in full-scale commercial CSP systems.

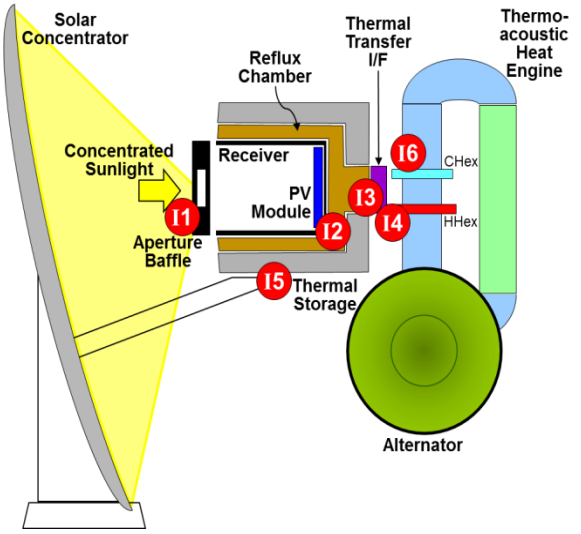

Figure 1 – Hybrid Solar Photovoltaic/ Thermoacoustic Power Converter System with Integrated Reflux Boiling/TES Heat Transport.

TES MATERIALS REVIEW

The majority of materials considered in the down selection process for the thermal energy storage (TES) phase change material (PCM) were included from the following reference web site: http://www.nrel.gov/docs/fy11osti/51446.pdf [13] using computer models to predict many properties of the mixtures described.

Safety is always a primary concern and it was important to remember that material compatibility and reactivity be considered regarding the boiling fluid, containment material, the TES PCM and its encapsulation material. These issues and concerns can be addressed but for first and/or early applications more chemically benign materials should be favored. For example, with naphthalene being a pure hydrocarbon and the baseline boiling and condensing transport fluid, some of the PCMs like the potential oxidizers containing nitrates and nitrites should be avoided, in case breaches in the containment materials were to occur. Safety concerns therefore provide constraints in the materials selection process. The chloride salts were preferred in this application since they tended to just dissolve in the naphthalene and if needed could be left behind as a salt if one were to simply distill the salt naphthalene mixture.

The selection of the TES PCM was constrained by a number of factors, including the naphthalene boiling/condensing fluid limitation where above 400 °C the degradation of the fluid becomes a factor due to the breaking down of the chemical bonds over time at temperature, which would result in more frequent replacement of the working fluid. Another high temperature constraint was the projected long-term operating temperature of the concentrator photovoltaic (CPV) cells which at the time were predicted to be about 350 °C. A system optimization of the CPV and thermoacoustic engine performance indicated it was best to operate at 350 °C and that the engine could perform well down to about 300 °C as the hot side or input temperature. Assuming it requires about a 10 °C temperature difference for the heat to be transferred into and out of the PCM, this means one is looking for material melting points in the range of approximately 310 to 340 °C. If one were constrained to use only one PCM, one would try to focus on materials at the higher end of this temperature range to try and maximize the efficiency of the engine, which occurs when the hot side temperature in closest to 350 °C. The following table 1 shows a list of example TES PCMs that fall within this melting point temperature range along with other properties.

Since a primary objective of the FOCUS program was to maximize the electrical power output for a given concentrator normal aperture area to the sun, a parabolic dish solar concentrator with a cavity receiver was selected to avoid the higher cosine and reradiating losses experience by parabolic troughs or other line focusing systems and power towers with heliostats. These dish systems have the challenge that if one places the added TES mass at the focus it increases the weight at the focus which impacts the structural cost of the parabolic dish. The added volume from TES at the focus can tend to block more of the aperture area if not properly addressed. The 15-minute requirement for buffer energy storage due to for example clouds passing was considered within the range of what could be easily incorporated at the dish focus assuming reasonable latent energy PCMs were selected. As required TES times increase, as they certainly will, the TES PCM and associated heat transport hardware will

Table 1 – List of examples of TES materials to be considered with their melting point, composition and theoretical latent heat [13].

Eutectic	Melting Point, C	Composition mol%	Theoretical Latent heat (J/g)
$FeCl_2$-NaCl-KCl	332	33.5-33.5-33.0	309
$FeCl_2$-NaCl-KCl	310	44.5-29.2-26.3	187
$FeCl_2$-NaCl-KCl	319	37.1-11.8-51.1	142
MgCl2-KCl-NaCl	331	34.4-65.7-25.1	198
Zn- Mg	340	52-48 wt%	180
CuCl- NaCl	314	73 - 27	-
CuCl- KCl	325	30 - 70	-
LiBr/KBr	328		333

certainly be incorporated into the existing pylons/pedestals support structure to minimize cost impacts to the systems. Dish and trough systems using flexible tubing to remove heat have been demonstrated in the past in industrial applications. A survey of the costs and availability of these TES PCMs revealed that the common metal chlorides like sodium chloride, potassium chloride and iron chloride used in the baseline PCM were commercially sold at low costs in quantities of metric tons. This results in an apparent economically viable solution to our baseline design TES challenge.

TEMPERATURE STAGING ANALYSIS

Figure 2 shows the system used with emphasis on the reflux boiler/TES system. The design parameters considered are the ambient temperature T_{amb}, the internal temperature of the system T_{int}, the solar flux q_{solar}, the output flux q_{rad} and q_{conv}, and the thermal energy storage E_g.

SYSTEM ENERGY ANALYSIS

The preliminary design of the reflux boiler/TES system (See Figure 2) was characterized and sized through a temperature-staging analysis based on a lumped-capacitance, thermal-energy-balance analysis described by Incropera and Dewitt [14]. The temperature vs. time response given by:

$$\frac{T-T_\infty}{T_i-T_\infty}=\exp(-at)+\frac{b/a}{T_i-T_\infty}[1-\exp(-at)] \qquad (1)$$

was the basic design metric and criteria in TE materials selection and sizing (i.e., mass and volume) (where T is the temperature, T_i is the initial temperature and T_∞ is the temperature when time $t\rightarrow\infty$, $a\equiv(h_s A_{s,c}/\rho Vc)$ and $b\equiv[(q_s'' A_{s,h}+\dot{E}_g/\rho Vc)]$ where h_s is the thermal convection coefficient of the system, $A_{s,c}$ is the

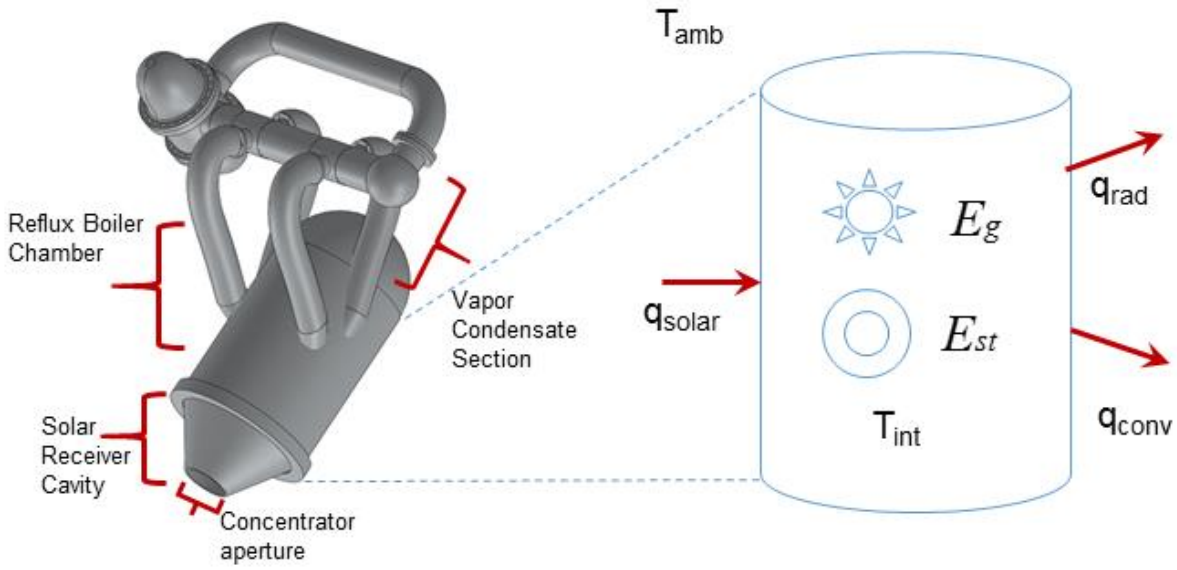

Figure 2 – Design of the reflux boiler/TES system with parameters considered for the analysis

California Institute of Technology. U.S. Government sponsorship acknowledged.

internal area, ρ is the density of the thermal energy storage material, V is the volume, c is the effective specific heat of the system (TES + structure), q''_s is the heat flux, $A_{s,h}$ is the outside heated area associated with q''_s, and $\dot{E}_g$ is the thermal energy storage value). This temperature – time relationship allows one to evaluate various scenarios of sensible heat absorption/dissipation and latent heat absorption/dissipation in the TES, while simultaneously accounting for energy transfer to the hot-side of the TAPC and chamber parasitic thermal losses. Judicious use of this equation in staged or phased analyses allows one to consider various TES temperature stages during heat-up and cool-down operation of the TES chamber; as part of a preliminary design sizing and thermal response analysis identifying the approximate thermal response of various TES material options. This allows one to identify and establish the basic reflux boiler/TES system design configuration and selected TES materials. More sophisticated finite element thermal/fluid dynamic analyses are planned in subsequent design phases to refine the design and the expected thermal/fluid dynamic response. In this analysis, the TAPC engine in Figure 1 is assumed to require 18 kW_{th} of thermal energy input for full power output. Several TES materials operating at 3 to 4 temperature stages between 300°C and 380°C were considered in this design analysis. In the temperature staging analysis, we consider the following scenario:

1) The 18 kW_{th} thermal engine is operating at a stabilized temperature of 350°C.
2) A cloud passes and blocks the solar input. The thermal engine keeps operating at 18 kW_{th} input and the temperature decreases until it reaches the melting temperature of the TES material. The reflux boiler contains sufficient TES material for 15 minutes of operation. The TES material is initially liquid and after 15 minutes, it has completely solidified and temperature keeps decreasing until it reaches 300 °C.
3) Once the temperature drops to 300 °C, the receiver is assumed to be back on sun and the temperature increases until it reaches the melting temperature of the TES material. At that point, the TES charges by liquefying while the temperature remains constant.

SYSTEM ENTROPY GENERATION ANALYSIS

The system entropy generation during the thermal storage process can be analyzed using the principles and concepts in Howell and Buckius [15] and Bejan [16]. The hybrid solar system design shown in Figures 1 and 2 incorporates the TES materials directly into the reflux boiler design; such that during the thermal storage process heat transfers directly from/to the reflux boiler medium (naphthalene) to the TES materials during discharging and charging. This work considers the naphthalene and TES materials starting from an initial temperature, Ti_i = 300 °C and heating to a final temperature T_f during the charging process, with latent heat transfer occurring isothermally at the TES phase change temperature, T_{TES}, (between T_i and T_f) during a constant temperature phase in the general heat up. The entropy generation during this thermal transfer is determined by considering both the naphthalene (N) and TES material entropy generation. It can be expressed by [15, 16]:

$$S_{gen,Naph} = S_{f,Naph} - S_{i,Naph} - \int_i^f \frac{dQ_N}{T} \qquad (2)$$

$$S_{gen,TES} = S_{f,TES} - S_{i,TES} - \int_i^f \frac{dQ_{TES}}{T} \qquad (3)$$

It is key to recognize that $dQ_N = -dQ_{TES}$ during the entire energy storage process, including any during isothermal latent phase change heat transfer into/out of TES materials. One can use entropy relations in Ref. [15], and neglecting pressure changes during the storage process (these are generally small enough to neglect), to arrive at:

$$S_{f,Naph} - S_{i,Naph} = m_{Naph} \cdot C_{p,Naph} \cdot \ln\left(\frac{T_{f,Naph}}{T_{i,Naph}}\right) \qquad (4)$$

$$S_{f,TES} - S_{i,TES} = m_{TES} \cdot C_{p,TES} \cdot \ln\left(\frac{T_{f,TES}}{T_{i,TES}}\right) \qquad (5)$$

The total entropy generation during the TES storage process is then [16]:

$$S_{gen,total} = S_{gen,Naph} + S_{gen,TES}$$

$$S_{gen,total} = m_{Naph} \cdot C_{p,Naph} \cdot \ln\left(\frac{T_{f,Naph}}{T_{i,Naph}}\right) \qquad (6)$$

$$+ m_{TES} \cdot C_{p,TES} \cdot \ln\left(\frac{T_{f,TES}}{T_{i,TES}}\right)$$

The implicit assumption in the above relationship is that $T_{f,Naph} \approx T_{f,TES}$ and that the temperature differential between the naphthalene and TES is negligibly small. If one accounts for the entropy generation associated with the heat transfer across a finite naphthalene-TES temperature differential, then an additional entropy

California Institute of Technology. U.S. Government sponsorship acknowledged.

generation must be added to the Eq. 6 relation according to the analysis of Bejan [16]:

$$S_{gen,HT} = \frac{\bar{h} \cdot A_{HT} \cdot \left(\Delta T_{Naph-TES}\right)^2}{T_{Naph}^2} \quad (7)$$

One important outcome from Eq. 6 is that lowering the final temperatures, $T_{f,Naph}$ and $T_{f,TES}$, generally lowers $S_{gen,total}$. Generally using phase change TES materials to absorb the thermal energy during isothermal phase change (with latent heat absorption) in the storage process accomplishes this objective. Latent phase change heat absorption and dissipation under isothermal conditions also closely mimics Carnot-like, reversible conditions, thereby minimizing entropy generation because the heat transfer occurs during an isothermal storage process and $(S_f - S_i)$ terms go to zero. Using multiple phase change TES materials at multiple isothermal phases at different temperatures during the heating can further help to minimize temperature increases during TES heat absorption process, which also lowers $S_{gen,total}$ [15, 16, 17] through Eq. 6. Furthermore, controlling and minimizing the $\Delta T_{naph-TES}$ during the heat transfer

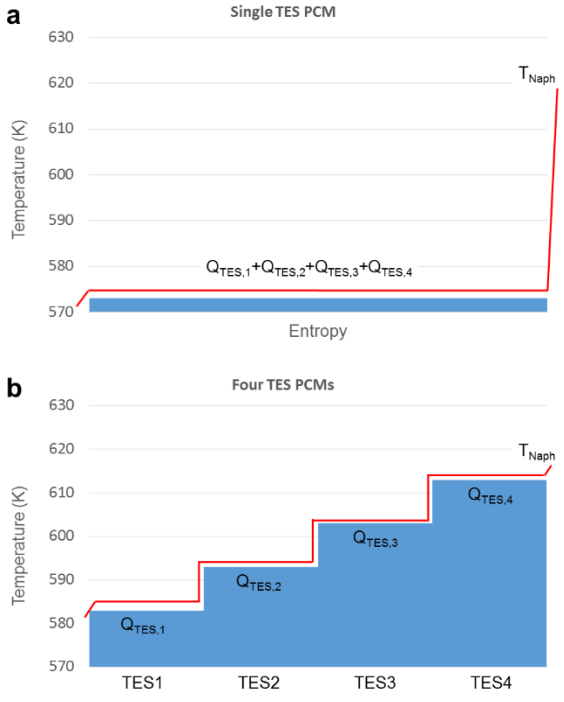

Figure 3 - TES Phase Change Material Comparison for (a) Single vs. (b) Multiple Materials

process as shown in Figure 3 also contributes to minimizing overall entropy generation in this system through Eq. 7. There are detailed proprietary aspects in the envisioned Reflux Boiler-TES design shown in Figure 2 that will accomplish this design objective.

RESULTS & PERFORMANCE CHARACTERISTICS

The thermal response analyses were initiated by simply considering three different TES materials individually in a "one-TES configuration" comprising the entire TES storage. The analysis is performed for the following three different TES materials with their different thermophysical properties from Table 1; $FeCl_2$ NaCl KCl, LiBr KBr, and $CaCl_2$ KCl LiCl. Figure 4 and Figure 5 represent the described scenario for 2 different solar thermal input conditions during the TES charge phases. In this system thermal analysis, the naphthalene-TES temperature differential, $\Delta T_{Naph-TES}$, is neglected as the envisioned detailed design is using special techniques to minimize this and thereby minimize the entropy generation (through Eq. 7). In Figure 4, we consider a 900 W thermal input with 300 W parasitic thermal loss. This corresponds to the excess of solar input compared to and over and above the 18 kWth thermal input to the TAPC engine. In the hybrid system in Figure 1, we oversize solar dish and receiver to provide the excess solar input to charge the TES system when needed and appropriate. This design oversizing is controlled by trading off cost and value of the dish/receiver design, TAPC design, and TES design to arrive at the most optimum Levelized Cost of Electricity (LCOE), while realizing that the TES enables and increases dispatchability. It is important to realize that this tradeoff is controlled by specific utility cost structures and what utility systems acutally provide peak power. The purpose here is not to delve into the details of this design tradeoff as it is beyond the scope of this work and analyses.

In Figure 4, LiBr KBr is the material that charges the fastest, but it takes 5.3 hour for the temperature to rise to the melting temperature of 327.8°C and 7.6 hours for the material to liquefy. That represents a total of almost 13 hours of storage charge time out of a potential full day of sun, which is untenable for one operational day of sun. Figure 3 also demonstrates that $FeCl_2$ NaCl KCl alone and $CaCl_2$ KCl LiCl alone take much longer than this to fully charge. This demonstrates that the excess-sun thermal input is too low in this case, and showing the need to have a certain level of excess-sun thermal input (>900 W) to make this thermal storage system viable. In Figure 5, we consider a case of 2025 W excess solar input over and above the 18kWth thermal input to the TAPC. In that case, the temperature rise time varies between 1.2 hours for LiBr KBr and 1.9 hours for $CaCl_2$ KCl LiCl. The liquefying is about 2.6 hours for all three TES materials. The reason why the liquefying time is

California Institute of Technology. U.S. Government sponsorship acknowledged.

equivalent for all three materials is because the amount of each material has been set for the same TES time, which is 15 minutes. The total TES charging time varies between 3.8 hours for LiBr KBr and 4.5 hours for $CaCl_2$ KCl LCl. These much shorter charge times are more realistic and viable for the expected operational day of sun in this CSP system. Based on the comparison we have done between the three TES materials, LiBr KBr is the one that gives the shortest charge time, but it is also the most expensive. Both $FeCl_2$ NaCl KCl alone and $CaCl_2$ KCl LiCl alone give slightly longer charge times, however they do provide more overall energy storage. Even though $FeCl_2$ NaCl KCl is not the material that gives the shortest charge time; it is the least expensive, creates a good amount of energy storage (almost as much as $CaCl_2$ KCl LiCl), and could therefore be the best compromise TES

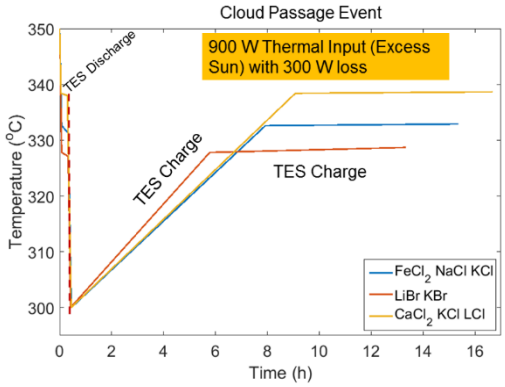

Figure 4 - TES thermal analysis showing a cloud passage event with 15 minutes TES discharge and TES charge with 900W excess sun thermal input. Overall system loss is 300W.

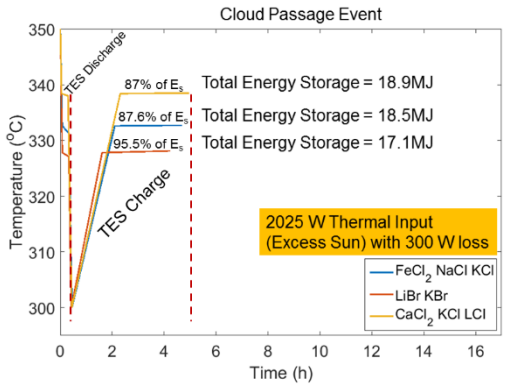

Figure 5 - TES thermal analysis showing a cloud passage event with 15 minutes TES discharge and TES charge with 2025W excess sun thermal input. Overall system loss is 300W.

candidate of the three considered here for a one-TES system.

In Figure 6, we repeat the same scenario we showed in Figure 4 and Figure 5. However, we split the 15-minute TES in three TES materials with different melting temperatures, essentially staging the energy storage at 3 different temperature levels during the overall charge process. The temperature-staged analysis used the three materials that are independently analyzed in Figure 4 and Figure 5. Using three materials with three different melting temperatures allows one to charge or discharge in incremental, isothermal steps. This allows the system to store / dissipate thermal energy at multiple Carnot-like, reversible stages as the Reflux boiler/TES system increases/decreases in temperature. This allows the extensive thermal energy storage shown in Figure 6 to occur for the minimum temperature excursions (increases/decreases), thereby minimizing the entropy generation given in Eq. 6, in addition to allowing the majority of the thermal storage energy transfer to mimic Carnot-like, reversible conditions (See Figure 3). This is one of the key entropy-generation-minimizing (or thermal-exergy-minimizing) features of this temperature-staged-TES approach, along with specialized design techniques to minimize $\Delta T_{Naph\text{-}TES}$ discussed above. This lowers the total thermal exergy loss in the round-trip charge/discharge process with 90% of the total energy storage in occurring in a isothermal phase change process in the PCM and achieving a higher ultimate storage temperature. This could even be extended to more stages, but benefits depend on specific TES system design, thermophysical properties and cost. During the course of the thermal analysis in Figure 6, it was recognized that there could additional benefits to consider a lower temperature TES material to operate in the temperature gap between 300°C and the first TES, LiBr/KBr, at 327.8°C. Table 2 shows the thermophysical properties of a fourth TES material, KNO_3/KCL, which is a lower temperature phase change material that would operate at 307.8°C. Table 2 compares its thermophysical properties with our initial three TES materials used in the Figure 5 analysis. The four TES materials are labeled with the notational scheme, TESn, where n indicates TES association given in Table 2.

An additional TES temperature-staged analysis was then performed to demonstrate the relative merits of using a fourth TES material and temperature stage, and comparing this to different numbers of temperature-stages in a cascaded TES system. Figure 7 shows the discharge/charge temperature profile associated with a four-stage TES material design. The

California Institute of Technology. U.S. Government sponsorship acknowledged.

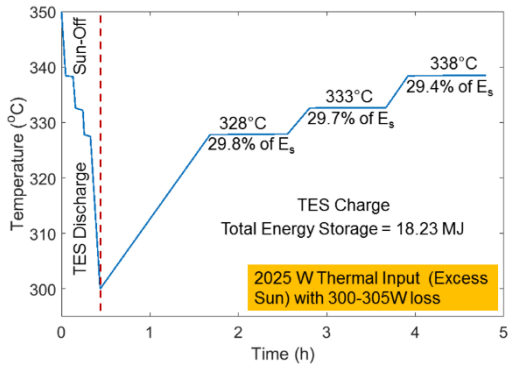

Figure 6 - Multiple Temperature-Stage Analysis showing TES discharge and charge for three TES materials.

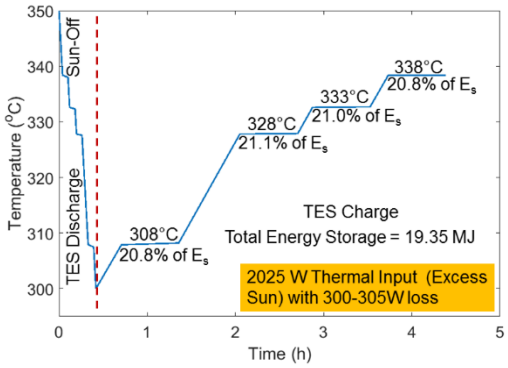

Figure 7 - Multiple Temperature-Staged Analysis showing TES discharge and charge for four TES materials.

Table 2 – List of TES materials used in this analysis with their thermal properties and masses to accommodate for 15 minutes of TES.

	KNO3/KCl TES1	LiBr KBr TES2	FeCl2 NaCl KCl TES3	CaCl2 KCl LiCl TES4
Melting Temp (C)	307.8	327.8	332.6	338.4
Latent Heat (J/kg)	105630	333000	308880	241200
Solid CCP (J/kg-K)	1156	562	1326	950
Liquid CCP (J/kg-K)	1177	672	1695	1200
Mass TES (kg)	152.6	49	52.5	68

Table 3 – Total energy stored, latent storage and highest storage temperature obtained for different combination scenarios of TES material using simultaneously 2, 3, or 4 of the TES materials from Table 2.

	Total Energy Stored (MJ)	Latent Heat Storage Fraction (%)	Highest Latent Storage Temperature Obtained	Latent Heat Entropy-Eq.7 (J/K)	Sensible Heat Entropy-Eq.6 (J/K)
TES 23	17.86	0.9107	332.6°C	0.083	6482
TES 34	18.83	0.8584	338.4°C	~0.1	7916
TES 234	18.23	0.8897	338.4°C	0.174	6716
TES 1234	19.35	0.8369	338.4°C	0.315	8164

energy storage at each temperature stage indicates how overall energy storage distributes throughout the intended discharge / charge process. Table 3 demonstrates with all four TES materials that the total energy stored is maximized with 19.35MJ. Using materials 2, 3, and 4, the total energy stored is lower with 18.23MJ, but the percentage latent storage is higher with 88.97%. If we use only materials 3 and 4, the total energy stored goes to 18.83 MJ, but the latent storage decreases to 85.84%. Finally, using only materials 2 and 3 gives the highest overall percentage latent storage with 91.07%, but it also stores the lowest amount of energy with 17.86MJ and has the lowest storage temperature of 332.6°C. Four temperature stages, using all four of the Table 2 TES materials, has the benefits of storing the most amount of total energy, while providing the highest ultimate storage temperature of all the temperature-staged storage configurations considered.

After about 4.5 hours, all four TES materials are fully charged with the excess solar thermal input shown in Figure 7. After that, temperature continues to increase until we reach the operating temperature threshold of 350°C in the Reflux Boiler. At 350°C, we partially close the concentrator aperture or adjust the solar reflector configuration to reduce the excess solar thermal input and thereby avoid system overheating.

Table 3 highlights the TES design optimization the must occur to arrive at the best system design, one of high thermal storage capability and low entropy generation. This investigation quantified the projected entropy generation for our four potential TES designs using Eqs. 6 and 7. These projected entropy generations include both the TES component and the naphthalene component as explicitly indicated in Eq. 6. Several major points are clear in Table 3. First, the entropy generation associated with latent heat processes are generally very small as they should be since we are storing energy in constant-temperature, Carnot-like processes. Second, the entropy generation in our designs is completely dominated by the entropy generation in sensible heat processes during the TES heating. One can see in Table 3 that there are two approximate minimum entropy points, one associated with our lower-temperature TES23 option and a higher-temperature TES234 option. The TES234 option allows the TES to store the higher total energy and operate (store energy) at the highest temperature nearest the Reflux Boiler/TES maximum temperature point of 350°C. The TES234 case is therefore the preferred design option in our current hybrid solar power system in Figure 1. The minimum entropy design cases can be explained by examining the fraction of Carnot, $\eta_{frac\text{-}Carnot}$, during the thermal energy storage process given by:

$$\eta_{frac-Carnot} = 1 - \frac{C_{p,TES} \cdot (T_f - T_i)}{h_{lat,TES}} - \left(\frac{m_{Naph}}{m_{TES}}\right) \cdot \left(\frac{C_{p,Naph}}{h_{lat,TES}}\right) \cdot \left(T_f - T_i\right) \quad (8)$$

Thermodynamic analysis of the energy storage process shows that this relationship defines the fraction of Carnot efficiency one can expect in the energy storage process, where T_i and T_f define the initial and final temperature conditions in the storage process. The storage process approaches a Carnot efficiency as $\eta_{frac\text{-}Carnot}$ approaches one. This Carnot fraction relation shows that the ratio of $C_{p,TES}$ to $h_{lat,TES}$ shown in Eq. 8 is a major controlling factor in determining the approach to Carnot efficiency and the lowest entropy cases. It turns out that the TES23 case and TES234 cases in Table 3 actually have the lowest ($C_{p,TES}$ / $h_{lat,TES}$) ratio, thereby giving those cases the highest fraction of Carnot during the thermal energy storage process, and therefore leading to the lowest entropy generation conditions. Two extreme cases were also investigated: TES2 (LiBr KBr) by itself and TES1 (KNO_3/KCl) by itself. In the TES2 case, the entropy generation analysis showed this option had the lowest entropy generation (sensible heat entropy generation 4717 J/K with negligible latent heat entropy generation) of all the cases investigated and Table 3 shows that this LiBr KBr material has the lowest ($C_{p,TES}/h_{lat,TES}$) of any materials studied herein. In the TES1 case, the entropy generation analysis showed this option had the highest entropy generation (sensible heat entropy generation >15500 J/K with negligible latent heat entropy generation) and Table 3 shows that this KNO_3/KCl has the highest ($C_{p,TES}$ / $h_{lat,TES}$) of the materials studied herein. This confirms the utility of Eq. 8 relation. The TES1 option has the additional issue of severe safety issues as they could react violently with the naphthalene in this design, while the TES2 option has the additional issue of prohibitive costs. These two issues complicated the TES materials selection process and led to dismissing the TES 1 material option completely for this energy storage design configuration. One final point to note is that trying to accomplish the magnitude of energy storage shown in Table 3 without any TES phase change material would lead to the maximum entropy generation due to the large required temperature changes associated sensible energy storage alone.

The third term of Eq. 8 also shows the dependence of the Carnot fraction on key design parameters unique to the combined, integrated Reflux Boiler/TES configuration investigated herein. The mass fraction, (m_{Naph}/m_{TES}) is a key parameter that decreases the Carnot fraction as (m_{Naph}/m_{TES}) increases. Therefore, this design approach desires to have higher TES mass and lower naphthalene mass to decrease exergy generation and approach Carnot-like processes. The ($C_{p,Naph}/h_{lat,TES}$) parameter is the second critical design parameter and plays the same role in reducing the Carnot fraction as the ($C_{p,TES}/h_{lat,TES}$) parameter discussed above. Lower ($C_{p,Naph}/h_{lat,TES}$) ratios increase the Carnot fraction and thereby lower the exergy generation, just as the ($C_{p,TES}/h_{lat,TES}$) parameter does. Eq. 8 can further be re-arranged to show the combined effect of these three terms in one:

$$\eta_{frac-Carnot} = 1 - \left[\frac{C_{p,TES}}{h_{lat,TES}} + \left(\frac{m_{Naph}}{m_{TES}}\right) \cdot \left(\frac{C_{p,Naph}}{h_{lat,TES}}\right)\right] \cdot \left(T_f - T_i\right) \quad (9)$$

One can clearly see that the combined property parameter in the second term of Eq. 9, associated with this integrated Reflux Boiler/TES design, collectively controls the Carnot fraction and the exergy generation.

California Institute of Technology. U.S. Government sponsorship acknowledged.

Minimizing this combined property parameter ultimately minimizes the exergy generation.

Table 3 analysis results also demonstrate that TES design configurations exhibiting high latent energy storage fractions are generally low entropy generation (i.e., low exergy) systems. This also aligns well with the characteristically low ($C_{p,TES}$ / $h_{lat,TES}$) ratios in low thermal exergy designs, as the latent heat storage tends to dominate the energy storage process. High latent energy storage fractions means the majority of thermal energy is being stored in isothermal latent heat absorption (and dissipation) processes, which are inherently low exergy, Carnot-like processes. These two characteristic metrics are therefore key inherent indicators of low exergy systems in this multiple TES design approach.

Finally, it is clear from analytic results in Table 3 that simply adding additional temperature stages in the energy storage process does not necessarily lead to lower entropy generation. The TES 234 case and TES 23 case show some of the lowest entropy generation cases, with TES 234 case having higher energy storage at higher temperatures closer to our storage temperature design requirement of 350°C. TES 234 storage configuration is the current preferred storage system design configuration for these reasons. TES 1234 case has higher entropy generation because the TES 1 materials in this temperature-staged storage configuration have the highest the ($C_{p,TES}$ / $h_{lat,TES}$) ratio of all the materials considered in this work, which therefore increases the entropy generation in this configuration. It is clear from this work that one must judiciously select proper TES materials to operate at the temperature stages of interest in this temperature-staged energy storage configuration to obtain optimum benefits. This TES optimization process is completely controlled by the ($C_{p,TES}$ / $h_{lat,TES}$) and ($C_{p,Naph}/h_{lat,TES}$) ratios, the (m_{Naph}/m_{TES}) ratio, the TES operating temperature of interest, and cost and safety of these different TES materials. The optimization process is then further constrained by the simple availability of various TES materials capable of operating at certain temperature ranges. Further research and development is required and planned to refine these low-exergy TES system design conclusions and approaches, then combining them with a rigorous cost analysis as discussed by Rezaei et al. [18] in a complete thermoeconomic analysis to establish a full picture of exergetic costs.

CONCLUSION

This work has identified a list of potential TES phase change materials that can satisfy the system thermal storage requirements in the hybrid solar photovoltaic/thermodynamic cycle power system shown in Figure 1. This work has down-selected TES materials that fit within the operational temperatures and requirements of the Hybrid Solar Photovoltaic/Thermoacoustic Power Converter system integrated with a low thermal-exergy-loss Reflux Boiling/TES Heat Transport sub-system. The system requirements compelled us to simulate different scenarios for 15-minutes cloud-driven thermal storage discharge event with either single TES materials at a time or a combination of up to 4 TES The analytic TES models and results demonstrated the benefits of combining several TES materials on the thermal storage sub-system characteristics and performance. The TES 234 case and TES 23 case show some of the lowest entropy generation cases, with TES 234 case having higher energy storage at higher temperatures closer to our storage temperature design requirement of 350°C. TES 234 storage configuration is the current preferred storage system design configuration for these reasons. Temperature staging of multiple TES materials does offer design and performance benefits as demonstrated in these analyses and results, however it does require judicious selection of the TES materials with close consideration and matching of their thermophysical properties and phase change temperatures. Thermal storage performance with multiple TES materials can store thermal energy at multiple temperature levels, thereby providing thermal exergy benefits, storing more thermal energy between set thermal limits, while providing higher ultimate storage temperatures, and providing a "thermal switch" capability to accommodate any runaway thermal excursions or extreme transients in Hybrid Solar Photovoltaic / Thermoacoustic Power Converter system. The TES optimization process is completely controlled by the ($C_{p,TES}/h_{lat,TES}$) and ($C_{p,Naph}/h_{lat,TES}$) ratios, the (m_{Naph}/m_{TES}) ratio, the TES operating temperature of interest, and cost and safety of these different TES materials, with lower ($C_{p,TES}/h_{lat,TES}$) and ($C_{p,Naph}/h_{lat,TES}$) ratios leading to lower entropy generation (lower exergy) designs. This TES optimization process is then tempered by the critically important cost and safety considerations of the various TES options. These initial system-level models and analyses have provided critical design sizing information and demonstrated key thermal performance sensitivities associated with the current hybrid power system. More research is required, with more detailed system-level models and analyses, to refine the internal thermal storage, internal thermal transport and thermal energy conversion characteristics and performance.

ACKNOWLEDGEMENTS

This work was carried out by the Department of Energy (DOE) through the ARPA-E FOCUS program

under award #DE-AR0000466 and under contract #DE-AR0000466 between NASA and the U.S. Department of Energy, Advanced Research Project Agency – Energy, Washington, DC at the Jet Propulsion Laboratory, California Institute of Technology, under a contract to the National Aeronautics and Space Administration.

REFERENCES

[1] Alpert, B. "Integrating CSP w/ TES into a Utility System" Phoenix: SunShot CSP Program Review. (2013).

[2] FULL-SPECTRUM OPTIMIZED CONVERSION AND UTILIZATION OF SUNLIGHT (FOCUS), U.S. Department of Energy, Advanced Research Projects Agency-Energy, Funding Opportunity Announcement (FOA) #DE-FOA-0000949, CFDA #81.135, (2013).

[3] Dunham, M. T. and Iverson, B. D., "High-efficiency thermodynamic power cycles for concentrated solar power systems", *Renewable and Sustainable Energy Reviews*, **30**, 758-770, http://dx.doi.org/10.1016/j.rser.2013.11.010, (2014).

[4] Denholm P., Wan Y.,-H., Hummon M., Mehos, M., "An Analysis of Concentrating Solar Power with Thermal Energy Storage in a California 33% Renewable Scenario", NREL/TP-6A20-58186, Golden, CO: National Renewable Energy Laboratory; (2013).

[5] Denholm P, Hand M. "Grid flexibility and storage required to achieve very high penetration of variable renewable electricity. *Energy Policy*, **39**: 1817–1830 (2011).

[6] Denholm P., Ela E., Kirby B., Milligan,M., "The role of energy storage with renewable electricity generation", NREL/TP-6A2-47187, Golden, CO: National Renewable Energy Laboratory; (2010).

[7] Sioshansi R., Denholm P., "The value of concentrating solar power and thermal energy storage", NREL-TP-6A2-45833, Golden, CO: National Renewable Energy Laboratory; (2010).

[8] Barlev D, Vidu R., Stroeve P., "Innovation in concentrated solar power", *Sol Energy Mater Sol Cells*, **95**: 2703–2725, (2011).

[9] Burgaleta Arias S., Ramirez D.J.I., "Gemasolar, the first tower thermosolar commercial plant with molten salt storage", In: Proceedings of SolarPACES 2011, Granada, Spain; September20–23, 2011.

[10] Kuravi, S., et al. (2013). "Thermal energy storage technologies and systems for concentrating solar power plants." *Progress in Energy and Combustion Science* **39**(4): 285-319.

[11] Stekli, J., et al. (2013). "Technical Challenges and Opportunities for Concentrating Solar Power With Thermal Energy Storage." *Journal of Thermal Science and Engineering Applications* **5**(2): 021011-021011.

[12] David E. Lee, Bill Nesmith, Terry Hendricks, Juan Cepeda-Rizo, Michael Petach, Emanuel Tward, Cecillia Penera, John Pohner, Scott Whitney, Jonathan Grandidier, "Efficient Heat Transfer Methods in a Hybrid Solar Thermal Power System for the FSPOT-X Project**",** *Proceedings of the ASME 2015 Power and Energy Conversion Conference (PowerEnergy2015)*, Paper #PowerEnergy2015-49658, San Diego, CA, July 2015.

[13] Gomez, J.C., (2011), "High-Temperature Phase Change Materials (PCM) Candidates for Thermal Energy Storage (TES) Applications", U.S. Department of Energy - National Renewable Energy Laboratory, Contract No. DE-AC36-08GO28308, Milestone Report NREL/TP-5500-51446, http://www.nrel.gov/docs/fy11osti/51446.pdf.

[14] Incropera, F. P. and Dewitt, D.P., (1990), **Fundamentals of Heat and Mass Transfer**, 3rd Ed., John Wiley & Sons, New York.

[15] Howell, J.R. and Buckius, (1987), R.O., **Fundamentals of Engineering Thermodynamics**, McGraw-Hill, Inc., New York.

[16] Bejan, A., (1996), **Entropy Generation Minimization: The Method of Thermodynamic Optimization of Finite-Size Systems and Finite-Time Processes**, CRC Press, Inc., Boca Raton.

[17] Kotze, J.P., (2014) "Thermal Energy Storage in Metallic Phase Change Materials" Doctoral Dissertation, Stellenbosch University, Matieland, South Africa, http://scholar.sun.ac.za.

[18] Rezaei, M., Anisur, M.R., Mahfuz, M.H., Kibria, M.A., Saidur, R., Metselaar, I.H.S.C., "Performance and cost analysis of phase change materials with different melting temperatures n heating systems", *Journal of Energy*, **53**: 173-178, Elsevier Ltd., (2013).